Lawrence Berkeley National Laboratory
LBL Publications

Title
A Method of Image-Based Aberration Metrology for EUVL Tools:

Permalink

Authors
Levinson, Zac
Raghunathan, Sudhar
Verduijn, Erik
et al.

Publication Date
2015-03-16

A Method of Image-Based Aberration Metrology for EUVL Tools

Zac Levinson[a], Sudhar Raghunathan[b], Erik Verduijn[b], Obert Wood[b], Pawitter Mangat[b], Kenneth Goldberg[c], Markus Benk[c], Antoine Wojdyla[c], Vicky Philipsen[d], Eric Hendrickx[d], Bruce W. Smith[a]

[a]Rochester Institute of Technology, 168 Lomb Memorial Drive, Rochester, NY 14623;
[b]GLOBALFOUNDRIES, 400 Stone Break Rd. Extension, Malta, NY, 12020;
[c]Lawrence Berkeley National Laboratory, One Cyclotron Road, Berkeley, CA 94720;
[d]IMEC, Kapeldreef 75, 3001 Heverlee, Belgium

ABSTRACT

We present an approach to image-based EUV aberration metrology using binary mask targets and iterative model-based solutions to extract both the amplitude and phase components of the aberrated pupil function. The approach is enabled through previously developed modeling, fitting, and extraction algorithms. We examine the flexibility and criticality of the method using two experimental case studies. The first extracts the pupil phase behavior from an ASML NXE:3100 exposure system and shows primary aberration sensitivity below 0.2 mλ. The second experiment extracts both components of the pupil function from the SHARP EUV microscope.

Keywords: EUV lithography, EUV aberrations, EUV transmission function, aberration metrology, image-based aberration metrology, pupil characterization

1. INTRODUCTION

For several lithography generations, pupil plane characterization has played a critical role in image process optimization.[1-3] This continues into EUV lithography (EUVL) with an additional importance placed on the understanding of the influences and variations to aberration behavior during system operation.[4] Optical interferometric methods have been shown to have sub-nanometer accuracy and are the de facto standard of aberration metrology.[5-7] Such methods can be challenging to implement during tool use though, especially where EUV wavelengths introduce additional constraints. To this end, we have developed a method at RIT to measure optical aberrations of an EUVL system from images formed by that system.[8-10]

Past studies, and traditional aberration theory in general, have focused on studying the pupil phase variation of imaging systems. This type of variation affects the shape of a point source travelling through the system, but does not account for other types of variation.[9, 11-13] These other types of system variation have generally been assumed to be small enough to not affect imaging, but have the potential to be important in EUV imaging. For example, even slightly misaligned lens elements can cause a variation in amplitude across the pupil.[14] This intensity imbalance can cause image variation through focus.[15, 16] For this reason we instead suggest a looser definition of aberrations: any system variation which impacts imaging.

We aim to both show that the RIT image-based method is flexible enough to account for this type of variation and use this method to explore the nature of amplitude variation in a real EUV imaging system. In this paper, we examine the flexibility and criticality of the method using two experimental case studies. The first is the characterization of an ASML NXE:3100 exposure system using SEM image analysis for inverse solutions of pupil plane phase behavior. The second study uses the SEMATECH High-NA Actinic Reticle review Project (SHARP)—an EUV mask microscope at Lawrence Berkeley National Laboratory—to study amplitude and phase pupil variation.[17, 18]
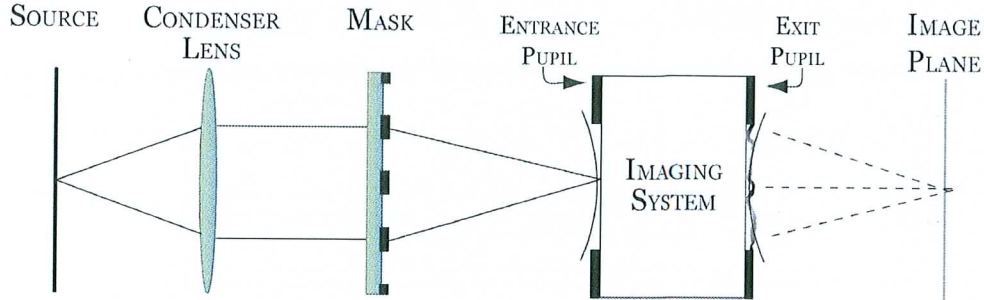
Figure 1. An example of the type of the type of imaging system being studied.

2. PRINCIPLES OF PUPIL VARIATION

2.1 Modeling pupil variation

We consider a general imaging system as shown in Figure 1. Light travelling from a point on the potentially extended source is imaged onto the mask. This light diffracts at the mask, creating a new wavefront that serves as the input of the imaging system. The system transforms that light in a unique way and outputs a new wavefront, which can vary in amplitude and phase from the ideal wavefront. In the ideal case the new wavefront converges to a point in the image plane.

The transfer of light through an optical system in the frequency domain can be given by Equation 1, where $\widetilde{E}(u,v)$ represents the frequency domain representation of $E(x,y)$—an electric field in the space domain—and $P(u,v)$ is called the pupil function.[19, 20] The coordinates u and v are normalized to λ/NA so that the pupil is defined by a unit circle. The pupil function describes the way the imaging system transforms the incoming electric field into the system output, and is what we seek to determine.

$$\widetilde{E_i}(u,v) = \widetilde{E_o}(u,v) \cdot P(u,v) \tag{1}$$

The pupil function is complex valued in general and can therefore be expressed in terms of its amplitude and phase, as in Equation 2.

$$P(u,v) = \alpha(u,v)e^{i\phi(u,v)} \tag{2}$$

Typically the amplitude function, $\alpha(u,v)$, is assumed to be equal to unity across the pupil. The phase function $\phi(u,v)$ is in units of radians in Equation 2, so it is customary to define a new function: $W(u,v) = \frac{\phi(u,v)}{2\pi}$ in units of waves, or a percentage of the actinic wavelength. These two functions both describe the phase difference between the object electric field and a Gaussian reference wavefront. In an ideal system this function is zero across the pupil at focus, and increases quadratically across the pupil through focus.[20, 21]

Traditionally, an imaging system is said to be aberrated when $W(u,v)$ is non-zero at focus. This phase function is difficult to measure directly though, so it is often useful to express $W(u,v)$ in an orthogonal function expansion. Strictly mathematically speaking, any basis function could be used to expand the phase function. It could be expanded in sinusoids of varying frequency—a Fourier series. It is well known, however, that the phase variation of an optical system is well described by Zernike polynomials.[11, 12, 21]

This choice of basis has two benefits: 1) a small number of terms are sufficient to describe the phase variation with minimal error, 2) each term has a direct physical interpretation. $W(u,v)$ expressed as a Zernike series is given by Equation 3, where ρ and θ are defined in Equation 4.

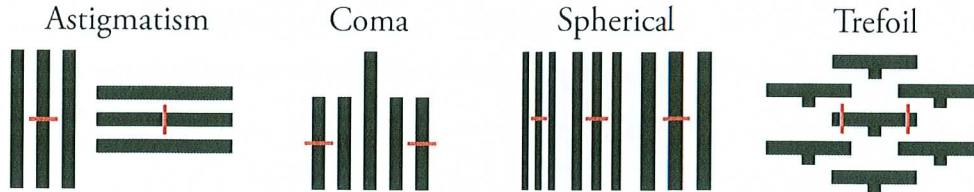$$W(u,v) = \sum_{n=0}^{\infty} a_n Z_n(\rho,\theta) \tag{3}$$

Figure 2. Examples of the binary metrology targets used for inverse wavefront interrogation. The lines normal to the pattern denote the measurement locations. Each type of aberration is interrogated by a difference between two structures.

$$\rho = \sqrt{u^2 + v^2} \tag{4a}$$

$$\theta = arctan(\frac{v}{u}) \tag{4b}$$

As previously mentioned, it is customary to assume that amplitude variations are small, and therefore negligible. We wish to investigate the nature of these amplitude variations, so we will not make this assumption. Instead, we define the amplitude variation to obey Equation 5.

$$\alpha(\rho, \theta) = \begin{cases} 1 + A(\rho, \theta) & : \rho \leq 1 \\ 0 & : \rho > 1 \end{cases} \tag{5}$$

The function $A(u, v)$ represents any additional amplitude or reduction in amplitude across the pupil. From here the analysis is identical to that of the pupil phase function: we wish to expand $A(u, v)$ in an orthogonal basis, though the most efficient basis is unknown at this point. Some authors have suggested expanding the entire pupil function in Zernike polynomials. This method has a number of restrictions though: 1) the pupil function must be azimuthally symmetric, 2) the expansion coefficients become complex valued.[22,23] We do not want to impose any *a priori* knowledge about the system, and we want to maintain ease of physical interpretation.

2.2 Extraction of pupil phase variation

At RIT we have developed a method to measure optical aberrations of an EUVL system from images formed by that system. Experimental measurements of aberration sensitive patterns are iteratively fit to PROLITH vector simulations to determine the wavefront variation.[24] We have used this technique successfully to characterize the phase variation of multiple EUVL systems and will present a brief summary of the method here. This method is covered in more detail in references 8–10.

We have identified a number of patterns that are most sensitive to a single aberration type, as seen in Figure 2. The lines orthogonal to the pattern in Figure 2 represent the measurement locations. These patterns are present on many masks so a special mask is often not necessary. These have been selected primarily so that there is a phase difference between measurement sites if a particular aberration is present. For example: the response used to estimate astigmatism is the difference in intensity between vertical and horizontal lines. Using the difference between structures provides an extremely robust aberration response.

The target sizes must be optimized for the specific exposure system and conditions however. We have found that there is an inherent trade-off between the printability and the aberration sensitivity of the target structures. Smaller structures are more sensitive to aberrations but the most sensitive structures may not resolve in resist. Targets are optimized by determining the system worst-case scenario—focus tolerance is set and aberration levels are estimated.[10] Aerial image simulations are run in these conditions and contours of constant normalized image log-slope (NILS) are drawn through the space. The appropriate targets can be determined by using a process dependent NILS threshold to define printability.

The image data used to extract the phase variation can be either in the form of an aerial image or in the form of CD measurements. After image data has been collected it is iteratively fit to aerial image simulations.
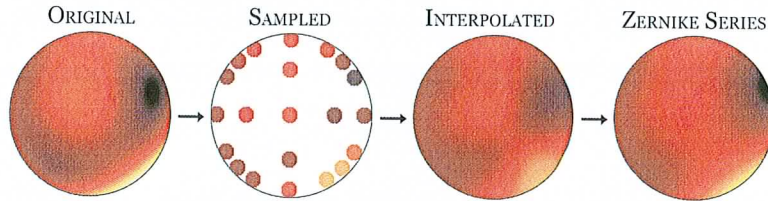
Figure 3. Flowchart of pupil amplitude reconstruction. First the pupil function is sampled via the diffracted spectrum of the targets used for phase interrogation. The value of these samples are determined via iterative fitting to aerial image simulations. Next Barnes analysis is used to interpolate between the samples to construct the original function. Finally, the interpolated function is expanded in a Fourier-Zernike series.

First an ideal wavefront is assumed then an analytic model is constructed for each target response. For example, a model is fit to the vertical-horizontal CD difference through focus and astigmatism. Finally the experimental data is fit to the analytical model to estimate the level of aberration. This process repeats for each target to obtain an initial guess for the wavefront, then the process repeats from the beginning.

2.2.1 Extraction of pupil amplitude variation

In the case of a coherent source, the diffracted energy from a line-space grating can be accurately approximated by a series of Bragg diffraction orders.[20, 21] The locations within the pupil of these spots of light can be predicted by Bragg's law, Equation 6, where ρ is as defined in Equation 4 and represents the relative frequency, λ is the actinic wavelength, P is the grating pitch, and NA is the system numerical aperture. The transfer of this diffracted energy through an imaging system can be modeled by its sampling the pupil function (as in Equation 1).

$$\rho = \frac{\lambda}{P \cdot NA} \tag{6}$$

In the partially coherent case analytic solutions prove considerably more difficult to obtain. Regardless, the partial coherence of the source can be thought of as averaging the pupil function in those locations.[21, 25, 26] In order to reconstruct the pupil amplitude function $A(u, v)$ image data is iteratively fit to simulations to determine the values of the average value of the function over each diffraction order. This value corresponds to the source-averaged sample of the pupil amplitude function. This algorithm is identical to that used to extract pupil phase with one complication: here the best choice of basis is unknown, so the source-averaged value of the amplitude function is determined for each diffraction order instead of an expansion coefficient.

This pupil sampling process is illustrated in Figure 3. The amplitude function can be reconstructed through interpolation after iteratively determining these samples. Barnes objective analysis is used to interpolate across the pupil between these samples.[27] This procedure—commonly used in metrological modeling—uses an initial guess for each grid point, then iteratively corrects it based on error computed from the known values. The weight of each error is proportional to the inverse of its distance from other points. This type of interpolation has the benefit of having high accuracy even when the samples are disordered and unevenly spaced. At this step the amplitude function has been determined, but it is useful to expand the interpolated function in an orthogonal basis. Zernike polynomials have been chosen in Figure 3 because of the *a priori* knowledge that the original function was composed in this basis.

This method is able to reproduce the original function with little error from a small number of samples. To illustrate this, 500 random amplitude functions composed of third-order Zernike amplitude polynomials (Z_A5-Z_A11) were sampled in the $\rho = 0.5$ and $\rho = 0.9$ pupil zones with a 0.1σ source. The mean range of the random functions was 19.09% of the pupil transmission deviation. These functions were then reconstructed using the scheme proposed in Figure 3. A histogram of the reconstructed function normalized RMS error (NRMSE) is given in Figure 4. The RMS of each initial function varied, so it would be inappropriate to directly compare the RMSE from these cases. Instead, the error was normalized to the range of the original function to facilitate comparison. This means that NRMSE is in units of percentage of the range. It can be seen in Figure 4 that
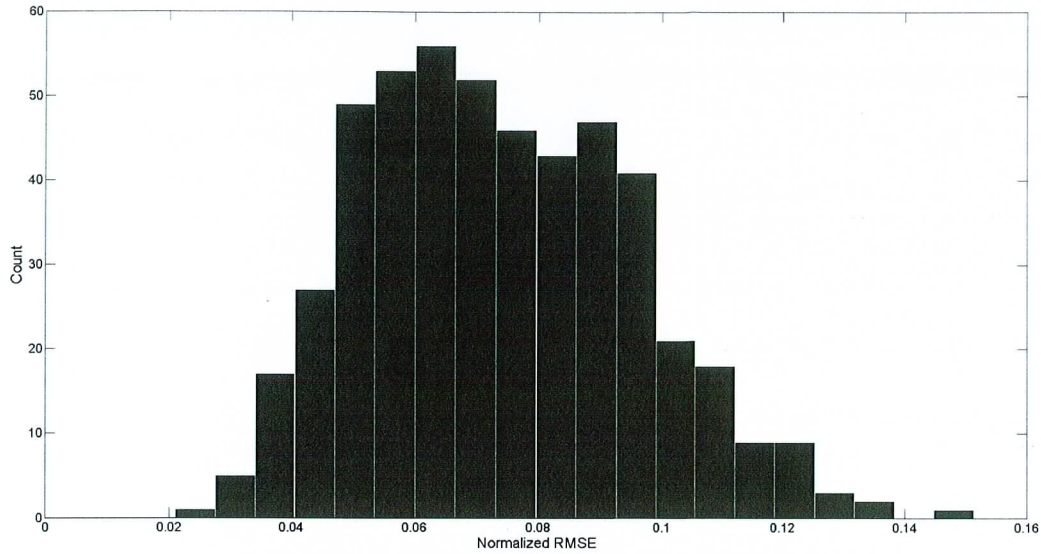
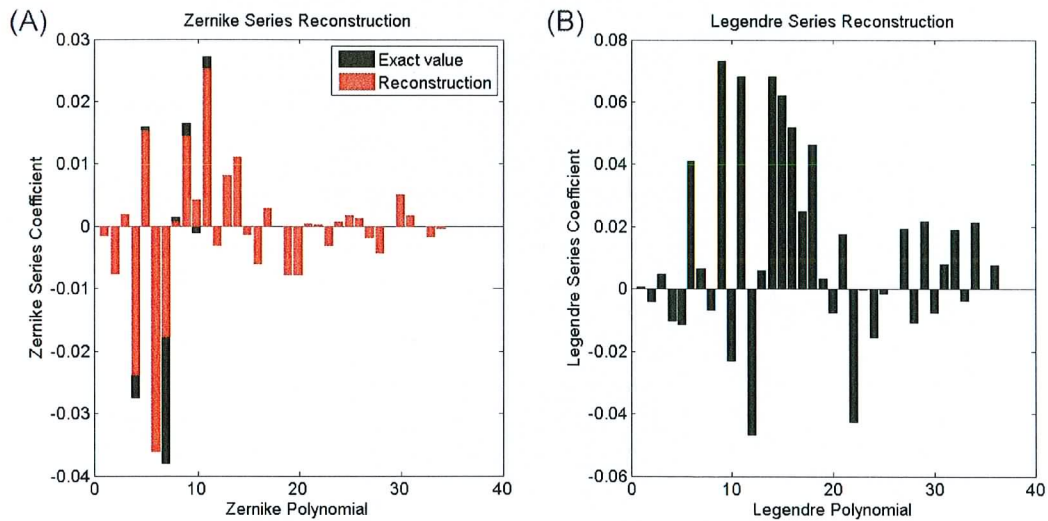Figure 4. Histogram of normalized RMSE for 500 different sampled and reconstructed pupils.

Figure 5. Comparison of an orthogonal function expansion of an interpolated amplitude function in a) Zernike polynomials, and b) the first 36 combinations of Cartesian Legendre polynomials.

the NRMSE closely follows a normal distribution with a mean of 7.08% of the range and a standard deviation of 1.96% of the range.

Visual inspection of Figure 3 shows that this error seems to manifest itself as a smoothing of the original function. This can be seen by comparing the extracted series coefficients for one of the reconstructed functions to the exact coefficient, Figure 5a. The original functions were composed of random arrangements of third-order Zernike polynomials, but higher order terms appear in the reconstructed function. This blurring effect is due to the pupil-averaging of the partially coherent source and can be reduced by increasing both the source coherence and the number of pupil samples. Still, the function can be reconstructed with little error with less than 36 terms. This is compared to an expansion in the first 36 combinations of Cartesian Legendre polynomials (Figure 5b) where the expansion would require more terms because the coefficients are still varying.

Table 1. CDs of the metrology targets used for wavefront extraction on the IMEC NXE:3100 system.

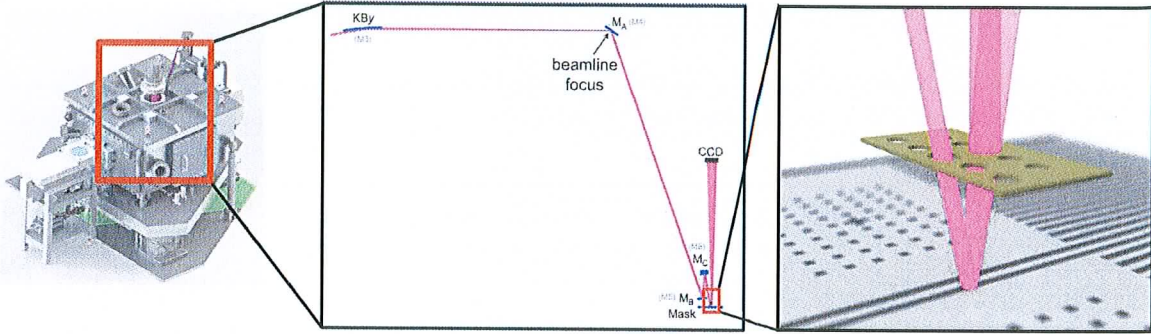| Aberration Name	Structure Type	Target CD [nm]
Astigmatism 90°	Vertical/Horizontal Line/Space	32
Astigmatism 45°	45°/135° Line/Space	32
Coma X	Vertical 5-bar	30
Coma Y	Horizontal 5-bar	30
Spherical	Line through pitch	20
Trefoil X	Horizontal T-Bar	35
Trefoil Y	Vertical T-Bar	35

Figure 6. A schematic view of the SHARP microscope at the Advanced Light Source. EUV light at 13.5 nm from a bending magnet is focused on the photomask. The photomask is imaged on a CCD sensor using Fresnel zone plate lens.

3. PROCEDURE

This work consists of two experimental case studies. One experiment was completed on an NXE:3100 exposure system to extract the pupil phase variation, while the other experiment was completed on the SHARP EUV mask microscope to extract pupil amplitude and phase variation. The expected sources of aberrations are different for each system due to the differences in image formation. Despite these differences, we extracted the aberrated pupil function of the imaging systems using a single algorithm.

3.1 NXE:3100 Phase Extraction

The target CDs of the structures used for this experiment are given in Table 1. These values were determined using the optimization procedure described in Section 2.2. A NILS threshold of 2.0 was used to define printability. Five exposures were completed on the IMEC NXE:3100 system. This system features a full field catoptric lens at 0.25NA. All exposures were completed with a $0.51\sigma_i$ - $0.8\sigma_o$ annular source. This source was chosen because, of the available sources, it was the most coherent source available.

The first two wafers were used to center the process window for the remaining wafers, which were used for wavefront extraction. Two of these remaining wafers were focus meanders, while the third was a FEM. CDs were measured using custom offline metrology software developed in MATLAB. Finally, the phase pupil variation was extracted from these CD measurements using custom software using the algorithm described in Section 2.2.

3.2 SHARP Amplitude and Phase Extraction

The SEMATECH Actinic Reticle Review Project (SHARP) is an EUV mask microscope at Lawrence Berkeley National Laboratory (LBNL). A schematic view of the system is shown in Figure 6. SHARP forms a magnified image of EUV masks onto a CCD sensor at 13.5 nm wavelength via interchangeable Fresnel zone plate lenses.

The target CDs of the structures used for this experiment are given in Table 2. These values were determined by calculating the pitch required to sample the desired pupil location. Structures were chosen to sample the

Table 2. CDs of the metrology targets used for pupil function extraction on SHARP.

Aberration Name	Structure Type	Target CD [nm]
Astigmatism 90°	Vertical/Horizontal Line/Space	30
Astigmatism 45°	45°/135° Line/Space	30
Coma X	Vertical 5-bar	50
Coma Y	Horizontal 5-bar	50
Spherical	Line through pitch	30
Trefoil X	Horizontal T-Bar	35
Trefoil Y	Vertical T-Bar	35

Figure 7. Examples of the CD-SEM micrographs used for CD measurements to extract the NXE:3100 aberrated wavefront.

$\rho =0.5$ and $\rho =0.9$ pupil zones. It is not necessary to balance sensitivity and printability on SHARP because the system records gray levels. Modulation is therefore not as important as when an image is formed in resist.

All data presented in this paper was collected using a 0.25 4xNA lens on July 28th, 2014. A 0.1σ conventional illuminator was chosen in order to resemble a coherent source, yet introduce a small amount of pupil averaging to decrease ringing effects. Each target was imaged through the full depth of focus at the smallest step available—$\pm 2.7\,\mu m$ in steps of $0.3\,\mu m$.

Images were analyzed in custom image processing software written in MATLAB. The images are aligned, interpolated, and finally averaged over a small area to form an approximation of the 1D aerial image. Images are collected through focus, so it is the through focus intensity volume that is used to extract the phase and amplitude functions in this case.

4. RESULTS AND DISCUSSION

4.1 NXE:3100 Phase Extraction

CD measurements were used to extract the NXE:3100 aberrated wavefront. These measurements were made offline from SEM micrographs of resist patterns. Examples of the resist patterns used in this experiment are given in Figure 7. There is a large amount of high frequency noise in the micrographs, which was filtered with a 4x4 pixel neighborhood median filter. A comparison of the original and filtered images is given in Figure 8a. The effect of the filter is more easily seen when comparing intensity line scans between the two images, Figure 8b. The CD measurements were then made from the filtered intensity profile.

A total of 10 iterations (totaling 20 minutes of runtime on a computer with a dual core Intel i7 processor and 8GB of RAM) were needed for the wavefront extraction models to converge on a solution. A plot of the final extracted wavefront is given in Figure 9. The wavefront has a total RMS of 13.4 mλ or 0.1809 nm. Exact values of the extracted Zernike coefficients are given in Table 3. The mean square error for the extraction model is also provided in Table 3. These values of error are consistent with past experimental results.[9, 28] Higher levels of error are present in the models to extract trefoil. It is suspected that this is due to both the difficulty in measuring this structure, as well as the relatively small exposure series used for extraction.

It is important to note that the ΔCD mean square error is not explicitly the error in the aberration extraction. There is no direct way to determine the error in aberration extraction because this is an inverse problem. The error reported here is the error in the model constructed for experimental ΔCD—the aberration extraction response—for each target type. This error is unavailable for spherical aberration because the response for this aberration type is not a difference in CD, but rather a best focus shift.
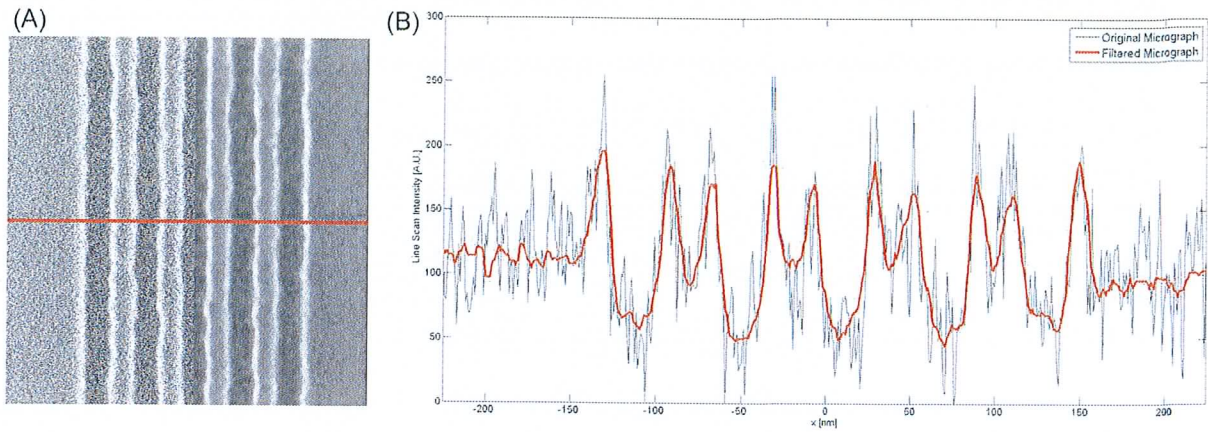
Figure 8. Example of SEM micrograph image processing for NXE:3100 case study. a) A comparison of the original (left) and median filtered (right) images, b) plot of a intensity line scan across the line in part (a) for both the original and filtered images.
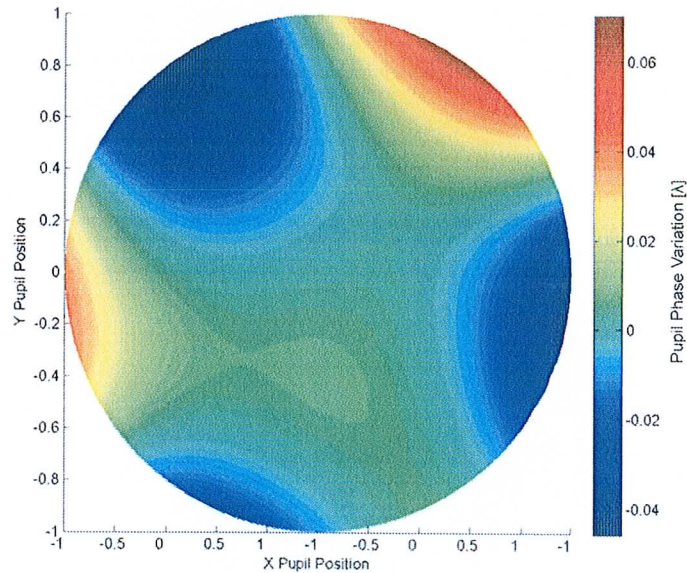

Figure 9. Pupil phase variation extracted from the IMEC NXE:3100 exposure system via the RIT image-based method.

Table 3. Extracted Zernike coefficients and ΔCD mean square error for the NXE:3100 after 10 iterations.

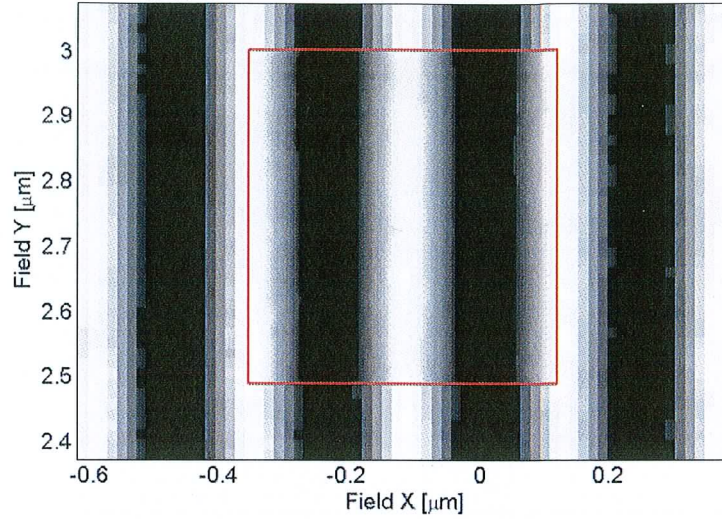| Aberration Name	Extracted Value [$m\lambda$]	ΔCD Mean Square Error [nm^2]
Astigmatism 90°	-0.82	0.136
Astigmatism 45°	+26.58	0.184
Coma X	-2.92	0.038
Coma Y	+12.00	0.043
Spherical	+0.15	N/A
Trefoil X	-36.09	1.032
Trefoil Y	+1.27	0.590

Figure 10. An example image from SHARP at the original resolution, and after Fourier interpolation (inset).
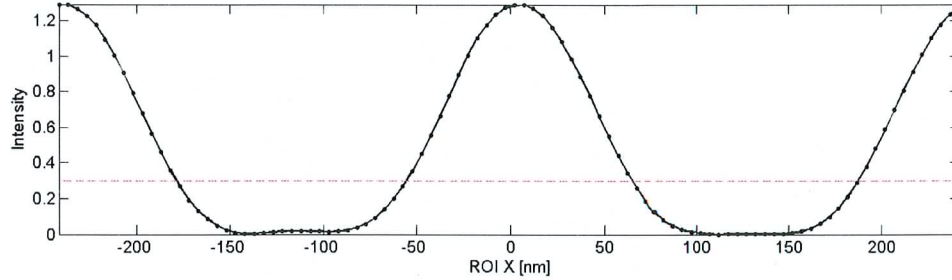

Figure 11. Column-wise average of the interpolated region in Figure 10 to estimate the pattern aerial image.

4.2 SHARP Amplitude and Phase Extraction

After data collection, images from SHARP were analyzed in custom image processing software. Dark current noise from the CCD was subtracted from the images, and then slight rotation and alignment errors were corrected. Next, the image was interpolated to a higher pixel grid, which also deconvolves the response of the CCD sensor. This process is shown in Figure 10. The images are collected at approximately 15 nm/px and were interpolated to approximately 5 nm/px. Finally, the interpolated region was averaged column-wise and normalized to obtain an approximate aerial image. The aerial image for the region interpolated in Figure 10 is shown in Figure 11. The white point and black point for normalization where chosen such that the intensity-focus volume peaked at the ideal value at best focus—1.29 for three beam imaging.

Examples of the images formed by SHARP for these experiments is given in Figure 12. A total of 8 iterations (totaling 18 hours of runtime on the same computer as in section 4.1) were needed for the wavefront extraction models to converge on a solution. A plot of the final extracted pupil amplitude function is given in Figure 13a, while the extracted pupil phase function is given in Figure 13b. The wavefront has a phase RMS of 61.3 mλ or 0.828 nm, and an amplitude RMS of 10% of the pupil transmission deviation with a range of 30% of the pupil transmission deviation. Exact values of the extracted phase Zernike coefficients are given in Table 4.

The SHARP pupil amplitude function was then expanded using Zernike amplitude polynomials (Z_A) and using Hermite amplitude polynomials (H_A), as in Figure 14. It is clear in Figure 14a that the Zernike amplitude coefficients are still varying significantly after 36 terms. On the other hand, it can be seen in Figure 14b that the amplitude function represented in a Hermite amplitude series results in approximately 15 terms. In this case the NRMSE of the Zernike series was 1.60%, compared to the 2.32% of the Hermite series. Regardless of the
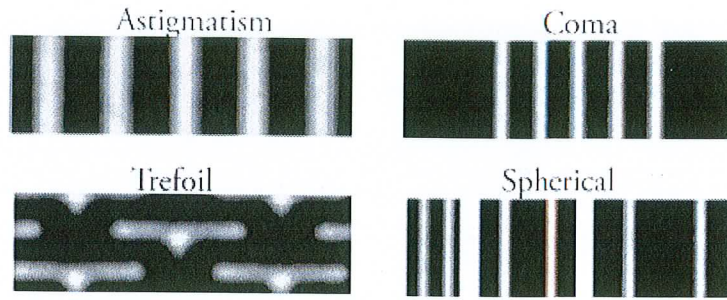
Figure 12. Examples of the SHARP micrographs used for aerial image measurements to extract the aberrated amplitude and phase functions.
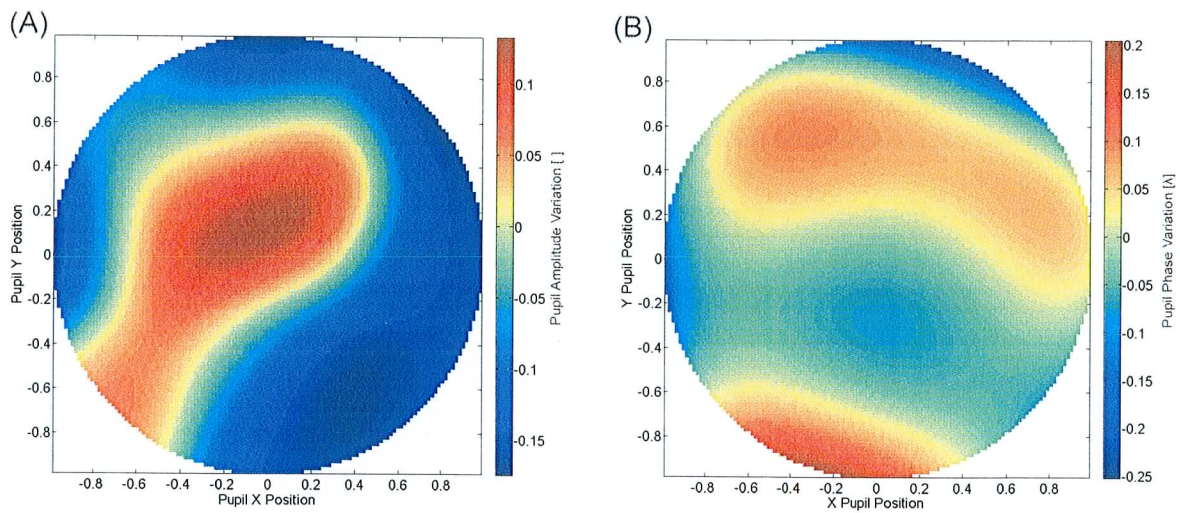

Figure 13. Pupil (a) amplitude variation, and (b) phase variation extracted from the LBNL SHARP EUV microscope via the RIT image-based method.

Table 4. Extracted Zernike coefficients and aerial image residual for SHARP after 8 iterations.

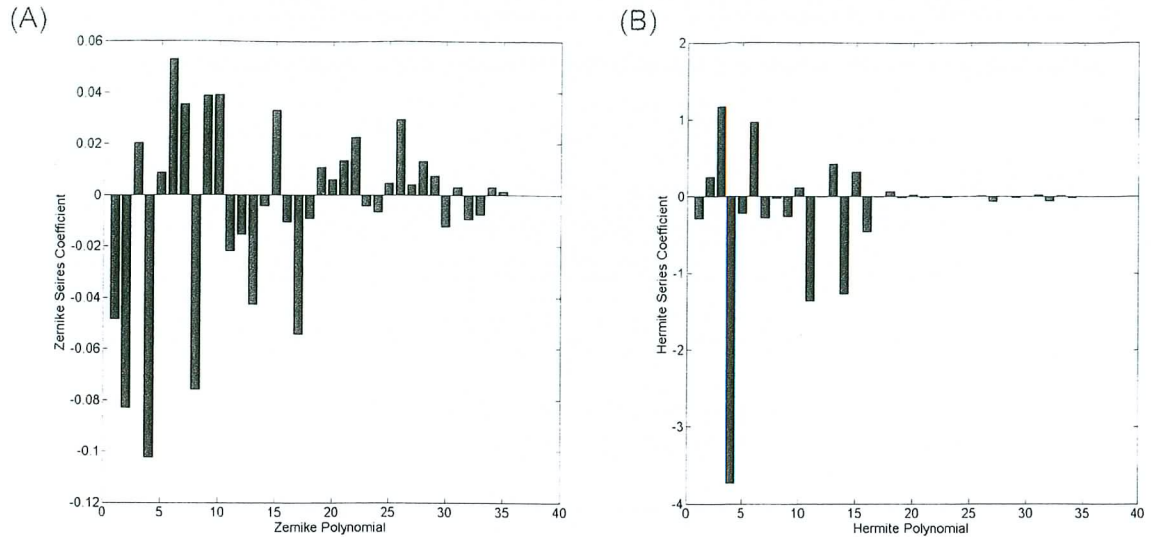| Aberration Name	Extracted Value $[m\lambda]$
Astigmatism 90°	-18.32
Astigmatism 45°	-1.20
Coma X	-6.56
Coma Y	-118.55
Spherical	-39.65
Trefoil X	+67.97
Trefoil Y	+92.16

(A)

(B)

Figure 14. SHARP pupil amplitude function expanded in two different orthognal basis. a) Zernike polynomials, b) Hermite polynomials.

slightly higher NRMSE the function appears to be better represented by Hermite polynomials. This is because the amplitude function mostly varies around zero-frequency, and most Zernike polynomials are zero at the origin.

5. CONCLUSIONS

We are developing a framework for extraction of both the amplitude and phase components of the pupil function of an EUVL system. This method uses the images formed by that system to extract its aberrated pupil function. We successfully demonstrated this technique in two different experiments. The first measured the pupil phase variation of an ASML NXE:3100 exposure system. We found a wavefront RMS of 13.4 mλ on this system. The second experiment measured the amplitude and phase pupil variation of the SHARP EUV mask microscope. We found an amplitude RMS of 10.18% and a phase RMS of 61.3 mλ. When expanding the SHARP pupil amplitude function in orthogonal series it was found that Hermite polynomials appear to describe pupil amplitude variation better than Zernike polynomials do. Future work will study this, and the other aspects of pupil amplitude variation, further. In addition, we will be working to reduce the 18 hour runtime associated with extracting amplitude variation.

ACKNOWLEDGMENTS

DISCLAIMER

This document was prepared as an account of work sponsored by the United States Government. While this document is believed to contain correct information, neither the United States Government nor any agency thereof, nor The Regents of the University of California, nor any of their employees, makes any warranty, express or implied, or assumes any legal responsibility for the accuracy, completeness, or usefulness of any information, apparatus, product, or process disclosed, or represents that its use would not infringe privately owned rights. Reference herein to any specific commercial product, process, or service by its trade name, trademark, manufacturer, or otherwise, does not necessarily constitute or imply its endorsement, recommendation, or favoring by the United States Government or any agency thereof, or The Regents of the University of California. The views and opinions of authors expressed herein do not necessarily state or reflect those of the United States Government or any agency thereof or The Regents of the University of California.